

# Generalized multiscale finite element methods for space-time heterogeneous parabolic equations

Eric T. Chung\*, Yalchin Efendiev†, Wing Tat Leung‡, Shuai Ye§

## Abstract

In this paper, we consider local multiscale model reduction for problems with multiple scales in space and time. We developed our approaches within the framework of the Generalized Multiscale Finite Element Method (GMsFEM) using space-time coarse cells. The main idea of GMsFEM is to construct a local snapshot space and a local spectral decomposition in the snapshot space. Previous research in developing multiscale spaces within GMsFEM focused on constructing multiscale spaces and relevant ingredients in space only. In this paper, our main objective is to develop a multiscale model reduction framework within GMsFEM that uses space-time coarse cells. We construct space-time snapshot and offline spaces. We compute these snapshot solutions by solving local problems. A complete snapshot space will use all possible boundary conditions; however, this can be very expensive. We propose using randomized boundary conditions and oversampling (cf. [3]). We construct the local spectral decomposition based on our analysis, as presented in the paper. We present numerical results to confirm our theoretical findings and to show that using our proposed approaches, we can obtain an accurate solution with low dimensional coarse spaces. We discuss using online basis functions constructed in the online stage and using the residual information. Online basis functions use global information via the residual and provide fast convergence to the exact solution provided a sufficient number of offline basis functions. We present numerical studies for our proposed online procedures. We remark that the proposed method is a significant extension compared to existing methods, which use coarse cells in space only because of (1) the parabolic nature of cell solutions, (2) extra degrees of freedom associated with space-time cells, and (3) local boundary conditions in space-time cells.

## 1 Introduction

Many multiscale processes vary over multiple space and time scales. These space and time scales are often tightly coupled. For example, flow processes in porous media can occur on multiple time scales over multiple spatial scales. Moreover, these scales can be non-separable. Reduced-order models for these problems require simultaneously treating spatial and temporal scales. Many previous approaches only handle spatial scales and spatial heterogeneities. These approaches have limitations when temporal heterogeneities arise. In this paper, we discuss a class of multiscale methods for handling space and time scales.

Some well-known approaches for handling *separable* spatial and temporal scales are homogenization techniques [26, 32, 33, 21]. In these methods, one solves local problems in space and time. To give an example, we consider a well-known case of the parabolic equation

$$\frac{\partial}{\partial t}u - \operatorname{div}(\kappa(x, x/\epsilon^\alpha, t, t/\epsilon^\beta)\nabla u) = f, \quad (1)$$

---

\*Department of Mathematics, The Chinese University of Hong Kong, Hong Kong SAR. This research is partially supported by the Hong Kong RGC General Research Fund (Project number: 400411).

†Department of Mathematics, Texas A&M University, College Station, TX; Numerical Porous Media SRI Center, King Abdullah University of Science and Technology (KAUST), Thuwal 23955-6900, Kingdom of Saudi Arabia

‡Department of Mathematics, Texas A&M University, College Station, TX.

§Department of Mathematics, Texas A&M University, College Station, TX.

subject to smooth initial and boundary conditions. Here,  $\epsilon$  is a small scale, and the spatial scale is  $\epsilon^\alpha$ , and the temporal scale is  $\epsilon^\beta$ . One can show that (e.g., [26, 32]), the homogenized equation has the same form as (1), but with the smooth coefficients  $\kappa^*(x, t)$ . One can compute the coefficients using the solutions of local space-time parabolic equations in the periodic cell. This localization is possible thanks to the scale separation. The local problems may or may not include time-dependent derivatives depending on the interplay between  $\alpha$  and  $\beta$  since the cell problems are independent of  $\epsilon$ . One can extend this homogenization procedure to numerical homogenization type methods [29, 1, 20, 23], where one solves the local parabolic equations in each coarse block and in each coarse time step. To compute the effective property, one averages the solutions of the local problems. These approaches work well in the scale separation cases, but do not provide accurate approximations when there is no scale separation.

Previous researchers developed a number of multiscale methods for solving space-time multiscale problems in the absence of scale separation. These approaches use Multiscale Finite Element Methods [24, 19, 27, 20], where one computes multiscale space-time basis functions, variational multiscale methods [25, ?], and other approaches [34, 35, 30, 28] that are developed for stabilization. In [31], Owhadi and Zhang proposed a novel approach that uses global space-time information in computing multiscale basis functions. All these approaches use only a limited number of basis functions (one basis function) in each coarse block. We note that there has been a large body of works in space-time finite element methods. In this paper, our objective is to develop a general approach that can systematically construct multiscale basis functions, and provide analysis for multiscale high-contrast problems.

Our approaches use the Generalized Multiscale Finite Element Method (GMsFEM) Framework and develop a systematic approach for identifying multiscale basis functions. The GMsFEM is a generalization of MsFEM, proposed by Hou and Wu [24]. The main idea of the GMsFEM is to construct multiscale basis functions by constructing snapshot spaces and performing local spectral decomposition in the snapshot spaces [16, 15, 5, 18, 6, 12, 18, 17, 18, 7, 10, 8, 9, 2]. The choice of the snapshot spaces and the local spectral decomposition is important for converging the resulting approach. We choose the snapshot spaces such that it can approximate the local solution space, while typically deriving local spectral decomposition from the analysis.

Previous approaches in developing multiscale spaces within GMsFEM focused on constructing multiscale spaces and relevant ingredients in space only. The proposed method is a significant extension compared to existing methods, which use coarse cells in space only because of (1) the parabolic nature of cell solutions, (2) extra degrees of freedom associated with space-time cells, and (3) local boundary conditions in space-time cells. In our approach, we construct snapshot spaces in space-time local domains. We construct the snapshot solutions by solving local problems. We can construct a complete snapshot space by taking all possible boundary conditions; however, this can result to very high computational cost. For this reason, we use randomized boundary conditions for local snapshot vectors by solving parabolic equations subject to random boundary and initial conditions. We compute only a few more than the number of basis functions needed. Computing multiscale basis functions employs local spectral problems. These local spectral problems are in space-time domain. Using space-time eigenvalue problems controls the errors associated with  $\partial u / \partial t$ . We discuss several choices for local spectral problems and present a convergence analysis of the method.

In the paper, we present several numerical examples. We consider the numerical tests with the conductivities that contain high contrast and these high conductivity regions move in time. These are challenging examples since the high-conductivity heterogeneities vary significantly during one coarse-grid time interval. If only using spatial multiscale basis functions, one will need a very large dimensional coarse space. In our numerical results, we use oversampling and randomized snapshots. Our results show that one can achieve a small error by selecting a few multiscale basis functions. The numerical results confirm our convergence analysis.

In the paper, we also discuss online multiscale basis functions. In [10, 9], we present an online procedure for *time-independent* problems. The main idea of online multiscale basis functions is to use the residual information and construct new multiscale basis functions adaptively. We would like to choose a number of offline basis functions such that with only 1-2 online iterations, we can substantially reduce the error. This requires a sufficient number of online basis functions, with the online basis function construction typically

derived by the analysis. In this paper, we present a possible online construction and show numerical results. Based on our previous results for *time-independent* problems, we show that one needs a sufficient number of offline basis functions to reduce the error substantially. In our numerical results, we observe a similar phenomena, i.e., the error decreases rapidly in 1-2 online iterations. We plan to investigate the convergence of the online procedure in our future work.

We organize the paper as follow. In Section 2, we present the underlying problem, the concepts of coarse and fine grids, the motivation of space-time approach, and the space-time GMsFEM framework. In Section 3, we present the convergence analysis for our proposed method. In Section 5, we present the new enrichment procedure of computing online multiscale basis functions. We present numerical results for offline GMsFEM and online GMsFEM in Section 4 and Section 6, separately. In Section 7, we draw conclusions.

## 2 Space-time GMsFEM

### 2.1 Preliminaries and motivation

Let  $\Omega$  be a bounded domain in  $\mathbb{R}^2$  with a Lipschitz boundary  $\partial\Omega$ , and  $[0, T]$  ( $T > 0$ ) be a time interval. In this paper, we consider the following parabolic differential equation

$$\begin{aligned} \frac{\partial}{\partial t}u - \operatorname{div}(\kappa(x, t)\nabla u) &= f && \text{in } \Omega \times (0, T), \\ u &= 0 && \text{on } \partial\Omega \times (0, T), \\ u(x, 0) &= \beta(x) && \text{in } \Omega, \end{aligned} \tag{2}$$

where  $\kappa(x, t)$  is a time dependent heterogeneous media (for example, a time dependent high-contrast permeability field),  $f$  is a given source function,  $\beta(x)$  is the initial condition. Our main objective is to develop space-time multiscale model reduction within GMsFEM and we use the time-dependent parabolic equation as an example. The proposed methods can be used for other models that require space-time multiscale model reduction.

We will introduce the space-time generalized multiscale finite element method in this section. The method follows the space-time finite element framework, where the time dependent multiscale basis functions are constructed on the coarse grid. Therefore, compared with the time independent basis structure, it gives a more efficient numerical solver for the parabolic problem in complicated media.

Before introducing our method, we need to define the mesh of the domain first. Let  $\mathcal{T}^h$  be a partition of the domain  $\Omega$  into fine finite elements where  $h > 0$  is the fine mesh size. Then we form a coarse partition  $\mathcal{T}^H$  of the domain  $\Omega$  such that every element in  $\mathcal{T}^H$  is a union of connected fine-mesh grid blocks, that is,  $\forall K_j \in \mathcal{T}^H$ ,  $K_j = \cup_{F \in I_j} F$  for some  $I_j \subset \mathcal{T}^h$ . The set  $\mathcal{T}^H$  is called the coarse grid and the elements of  $\mathcal{T}^H$  are called coarse elements. Moreover,  $H > 0$  is the coarse mesh size. In this paper, we consider rectangular coarse elements for the ease of discussions and illustrations. The methodology presented can be easily extended to coarse elements with more general geometries. Let  $\{x_i\}_{i=1}^{N_c}$  be the set of nodes in the coarse grid  $\mathcal{T}^H$  (or coarse nodes for short), where  $N_c$  is the number of coarse nodes. We denote the neighborhood of the node  $x_i$  by

$$\omega_i = \bigcup \{K_j \in \mathcal{T}^H : x_i \in \overline{K_j}\}.$$

Notice that  $\omega_i$  is the union of all coarse elements  $K_j \in \mathcal{T}^H$  sharing the coarse node  $x_i$ . An illustration of the above definition is shown in Figure 1. Next, let  $\mathcal{T}^T = \{(T_{n-1}, T_n) | 1 \leq n \leq N\}$  be a coarse partition of  $(0, T)$  where

$$0 = T_0 < T_1 < T_2 < \dots < T_N = T$$

and we define a fine partition of  $(0, T)$ ,  $\mathcal{T}^t$  by refining the partition  $\mathcal{T}^T$ .

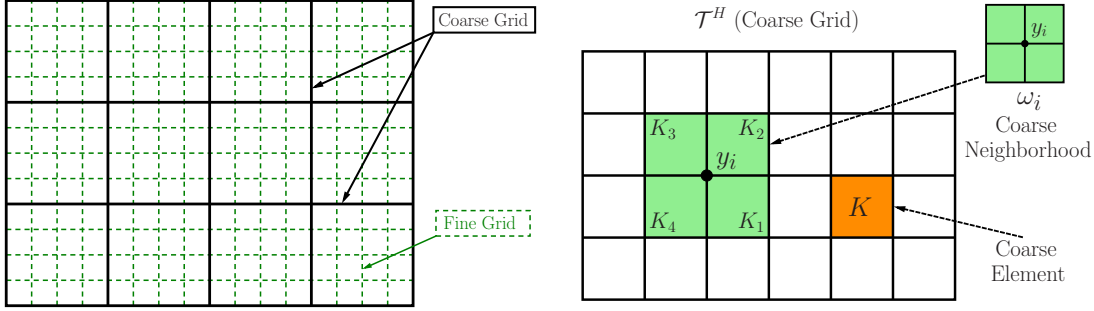


Figure 1: Left: an illustration of fine and coarse grids. Right: an illustration of a coarse neighborhood and a coarse element.

To fix the notations, we will use the standard conforming piecewise linear finite element method for the computation of the fine-scale solution. One can use discontinuous Galerkin coupling also [22, 13, 14]. Specifically, we define the finite element space  $V_h$  with respect to  $\mathcal{T}^h \times (0, T)$  as

$$V_h = \{v \in L^2((0, T); C^0(\Omega)) \mid v = \phi(x)\psi(t) \text{ where } \phi|_K \in Q_1(K) \forall K \in \mathcal{T}^h, \psi|_\tau \in C^0(\tau) \forall \tau \in \mathcal{T}^T \text{ and } \psi|_\tau \in P_1(\tau) \forall \tau \in \mathcal{T}^t\},$$

then the fine-scale solution  $u_h \in V_h$  is obtained by solving the following variational problem

$$\int_0^T \int_\Omega \frac{\partial u_h}{\partial t} v + \int_0^T \int_\Omega \kappa \nabla u_h \cdot \nabla v + \sum_{n=0}^{N-1} \int_\Omega [u_h(x, T_n)] v(x, T_n^+) = \int_0^T \int_\Omega f v + \int_\Omega \beta(x) v(x, T_0^+), \quad \forall v \in V_h, \quad (3)$$

where  $[\cdot]$  is the jump operator such that

$$\begin{cases} [u_h(x, T_n)] = u_h(x, T_n^+) - u_h(x, T_n^-) & \text{for } n \geq 1, \\ [u_h(x, T_n)] = u_h(x, T_0^+) & \text{for } n = 0. \end{cases}$$

We assume that the fine mesh size  $h$  is small enough so that the fine-scale solution  $u_h$  is close enough to the exact solution. The purpose of this paper is to find a multiscale solution  $u_H$  that is a good approximation of the fine-scale solution  $u_h$ .

Now we present the general idea of GMsFEM. We will use the space-time finite element method to solve problem (2) on the coarse grid. That is, we find  $u_H \in V_H$  such that

$$\int_0^T \int_\Omega \frac{\partial u_H}{\partial t} v + \int_0^T \int_\Omega \kappa \nabla u_H \cdot \nabla v + \sum_{n=0}^{N-1} \int_\Omega [u_H(x, T_n)] v(x, T_n^+) = \int_0^T \int_\Omega f v + \int_\Omega \beta(x) v(x, T_0^+), \quad \forall v \in V_H, \quad (4)$$

where  $V_H$  is the multiscale finite element space which will be introduced in the following subsections.

The computational cost for solving the equation (4) is huge since we need to compute the solution  $u_H$  in the whole time interval  $(0, T)$  at one time. In fact, if we assume the solution space  $V_H$  is a direct sum of the spaces only containing the functions defined on one single coarse time interval  $(T_{n-1}, T_n)$ , we can decompose the problem (4) into a sequence of problems and find the solution  $u_H$  in each time interval sequentially. Our coarse space will be constructed in each time interval and we will have

$$V_H = \oplus_{n=1}^N V_H^{(n)},$$

where  $V_H^{(n)}$  only contains the functions having zero values in the time interval  $(0, T)$  except  $(T_{n-1}, T_n)$ , namely  $\forall v \in V_H^{(n)}$ ,

$$v(\cdot, t) = 0 \text{ for } t \in (0, T) \setminus (T_{n-1}, T_n).$$

The equation (4) can be decomposed into the following problem: find  $u_H^{(n)} \in V_H^{(n)}$  (where  $V_H^{(n)}$  will be defined later) satisfying

$$\begin{aligned} & \int_{T_{n-1}}^{T_n} \int_{\Omega} \frac{\partial u_H^{(n)}}{\partial t} v + \int_{T_{n-1}}^{T_n} \int_{\Omega} \kappa \nabla u_H^{(n)} \cdot \nabla v + \int_{\Omega} u_H^{(n)}(x, T_{n-1}^+) v(x, T_{n-1}^+) \\ & = \int_{T_{n-1}}^{T_n} \int_{\Omega} f v + \int_{\Omega} g_H^{(n)}(x) v(x, T_{n-1}^+), \quad \forall v \in V_H^{(n)}, \end{aligned} \quad (5)$$

where

$$g_H^{(n)}(\cdot) = \begin{cases} u_H^{(n-1)}(\cdot, T_{n-1}^-) & \text{for } n \geq 1, \\ \beta(\cdot) & \text{for } n = 0. \end{cases}$$

Then, the solution  $u_H$  of the problem (4) is the direct sum of all these  $u_H^{(n)}$ 's, that is  $u_H = \bigoplus_{n=1}^N u_H^{(n)}$ .

Next, we motivate the use of space-time multiscale basis functions by comparing it to space multiscale basis functions. In particular, we discuss the savings in the reduced models when space-time multiscale basis functions are used compared to space multiscale basis functions. We denote  $\{t_{n1}, \dots, t_{np}\}$  are  $p$  fine time steps in  $(T_{n-1}, T_n)$ . When we construct space-time multiscale basis functions, the solution can be represented as  $u_H^{(n)} = \sum_{l,i} c_{l,i} \psi_l^{\omega_i}(x, t)$  in the interval  $(T_{n-1}, T_n)$ . In this case, the number of coefficients  $c_{l,i}$  is related to the size of the reduced system in space-time interval. On the other hand, if we use only space multiscale basis functions, we need to construct these multiscale basis functions at each fine time instant  $t_{nj}$ , denoted by  $\psi_l^{\omega_i}(x, t_{nj})$ . The solution  $u_H$  spanned by these basis functions will have a much larger dimension because each time instant is represented by multiscale basis functions. Thus, performing space-time multiscale model reduction can provide a substantial CPU savings.

In the next, we will discuss space-time multiscale basis functions. First, we will construct multiscale basis functions in the offline mode without using the residual. Next, in Section 5, we will discuss online space-time multiscale basis construction.

## 2.2 Construction of offline basis functions

### 2.2.1 Snapshot space

Let  $\omega$  be a given coarse neighborhood in space. We omit the coarse node index to simplify the notations. The construction of the offline basis functions on coarse time interval  $(T_{n-1}, T_n)$  starts with a snapshot space  $V_{\text{snap}}^{\omega}$  (or  $V_{\text{snap}}^{\omega(n)}$ ). We also omit the coarse time index ( $n$ ) to simplify the notations. The snapshot space  $V_{\text{snap}}^{\omega}$  is a set of functions defined on  $\omega$  and contains all or most necessary components of the fine-scale solution restricted to  $\omega$ . A spectral problem is then solved in the snapshot space to extract the dominant modes in the snapshot space. These dominant modes are the offline basis functions and the resulting reduced space is called the offline space. There are two choices of  $V_{\text{snap}}^{\omega}$  that are commonly used.

The first choice is to use all possible fine-grid functions in  $\omega \times (T_{n-1}, T_n)$ . This snapshot spaces provide accurate approximation for the solution space; however, this snapshot space can be very large. The second choice for the snapshot spaces consists of solving local problems for all possible boundary conditions. In particular, we define  $\psi_j$  as the solution of

$$\begin{aligned} & \frac{\partial}{\partial t} \psi_j - \text{div}(\kappa(x, t) \nabla \psi_j) = 0 \quad \text{in } \omega \times (T_{n-1}, T_n), \\ & \psi_j(x, t) = \delta_j(x, t) \quad \text{on } \partial(\omega \times (T_{n-1}, T_n)). \end{aligned} \quad (6)$$

Here  $\delta_j(x, t)$  is a fine-grid delta function and  $\partial(\omega \times (T_{n-1}, T_n))$  denotes the boundaries  $t = T_{n-1}$  and on  $\partial\omega \times (T_{n-1}, T_n)$ . In general, the computations of these snapshots are expensive since in each local coarse neighborhood  $\omega$ ,  $O(M_n^{\partial\omega})$  number of local problems are required to be solved. Here,  $M_n^{\partial\omega}$  is the number of fine grids on the boundaries  $t = T_{n-1}$  and on  $\partial\omega \times (T_{n-1}, T_n)$ . A smaller yet accurate snapshot space is needed to build a more efficient multiscale method. We can take an advantage of randomized oversampling

concepts [4] and compute only a few snapshot vectors, which will reduce the computational cost remarkably while keeping required accuracy. Next, we introduce randomized snapshots.

Firstly, we introduce the notation for oversampled regions. We denote by  $\omega^+$  the oversampled space region of  $\omega \subset \omega^+$ , defined by adding several fine- or coarse-grid layers around  $\omega$ . Also, we define  $(T_{n-1}^*, T_n)$  as the left-side oversampled time region for  $(T_{n-1}, T_n)$ . In the following, we generate inexpensive snapshots using random boundary conditions on the oversampled space-time region  $\omega^+ \times (T_{n-1}^*, T_n)$ . That is, instead of solving Equation (6) for each fine boundary node on  $\partial(\omega \times (T_{n-1}, T_n))$ , we solve a small number of local problems imposed with random boundary conditions

$$\begin{aligned} \frac{\partial}{\partial t} \psi_j^+ - \operatorname{div}(\kappa(x, t) \nabla \psi_j^+) &= 0 \quad \text{in } \omega^+ \times (T_{n-1}^*, T_n), \\ \psi_j^+(x, t) &= r_l \quad \text{on } \partial(\omega^+ \times (T_{n-1}^*, T_n)), \end{aligned}$$

where  $r_l$  are independent identically distributed (i.i.d.) standard Gaussian random vectors on the fine-grid nodes of the boundaries  $t = T_{n-1}^*$  and on  $\partial\omega^+ \times (T_{n-1}^*, T_n)$ . Then the local snapshot space on  $\omega^+ \times (T_{n-1}^*, T_n)$  is

$$V_{\text{snap}}^{\omega^+} = \operatorname{span}\{\psi_j^+(x, t) | j = 1, \dots, L^\omega + p_{\text{bf}}^\omega\},$$

where  $L^\omega$  is the number of local offline basis we want to construct in  $\omega$  and  $p_{\text{bf}}^\omega$  is the buffer number. Later on, we use the same buffer number for all  $\omega$ 's and simply use the notation  $p_{\text{bf}}$ . In the following sections, if we specify one special coarse neighborhood  $\omega_i$ , we use the notation  $L_i$  to denote the number of local offline basis. With these snapshots, we follow the procedure in the following subsection to generate offline basis functions by using an auxiliary spectral decomposition.

### 2.2.2 Offline space

To obtain the offline basis functions, we need to perform a space reduction by appropriate spectral problems. Motivated by our later convergence analysis, we adopt the following spectral problem on  $\omega^+ \times (T_{n-1}, T_n)$ :

Find  $(\phi, \lambda) \in V_{\text{snap}}^{\omega^+} \times \mathbb{R}$  such that

$$A_n(\phi, v) = \lambda S_n(\phi, v), \quad \forall v \in V_{\text{snap}}^{\omega^+}, \quad (7)$$

where the bilinear operators  $A_n(\phi, v)$  and  $S_n(\phi, v)$  are defined by

$$\begin{aligned} A_n(\phi, v) &= \frac{1}{2} \left( \int_{\omega^+} \phi(x, T_n) v(x, T_n) + \int_{\omega^+} \phi(x, T_{n-1}) v(x, T_{n-1}) \right) + \int_{T_{n-1}}^{T_n} \int_{\omega^+} \kappa(x, t) \nabla \phi \cdot \nabla v, \\ S_n(\phi, v) &= \int_{\omega^+} \phi(x, T_{n-1}) v(x, T_{n-1}) + \int_{T_{n-1}}^{T_n} \int_{\omega^+} \tilde{\kappa}^+(x, t) \phi v, \end{aligned} \quad (8)$$

where the weighted function  $\tilde{\kappa}^+(x, t)$  is defined by

$$\tilde{\kappa}^+(x, t) = \kappa(x, t) \sum_{i=1}^{N_c} |\nabla \chi_i^+|^2,$$

$\{\chi_i^+\}_{i=1}^{N_c}$  is a partition of unity associated with the oversampled coarse neighborhoods  $\{\omega_i^+\}_{i=1}^{N_c}$  and satisfies  $|\nabla \chi_i^+| \geq |\nabla \chi_i|$  on  $\omega_i$  where  $\chi_i$  is the standard multiscale basis function for the coarse node  $x_i$  (that is, with linear boundary conditions for cell problems). More precisely,

$$\begin{aligned} -\operatorname{div}(\kappa(x, T_{n-1}) \nabla \chi_i) &= 0, \quad \text{in } K \in \omega_i, \\ \chi_i &= g_i, \quad \text{on } \partial K, \end{aligned} \quad (9)$$

for all  $K \in \omega_i$ , where  $g_i$  is a continuous function on  $\partial K$  and is linear on each edge of  $\partial K$ .

We arrange the eigenvalues  $\{\lambda_j^+ | j = 1, 2, \dots, L^\omega + p_{\text{bf}}^\omega\}$  from (7) in the ascending order, and select the first  $L^\omega$  eigenfunctions, which are corresponding to the first  $L^\omega$  ordered eigenvalues, and denote them by  $\{\Psi_1^{\omega^+, \text{off}}, \dots, \Psi_{L^\omega}^{\omega^+, \text{off}}\}$ . Using these eigenfunctions, we can define

$$\psi_j^{\omega^+}(x, t) = \sum_{k=1}^{L^\omega + p_{\text{bf}}^\omega} (\Psi_j^{\omega^+, \text{off}})_k \psi_k^+(x, t), \quad j = 1, 2, \dots, L^\omega,$$

where  $(\Psi_j^{\omega^+, \text{off}})_k$  denotes the  $k$ -th component of  $\Psi_j^{\omega^+, \text{off}}$ , and  $\psi_k^+(x, t)$  is the snapshot basis function computed on  $\omega^+ \times (T_{n-1}^*, T_n)$  as in the previous subsection. Then we can obtain the snapshots  $\psi_j^\omega(x, t)$  on the target region  $\omega \times (T_{n-1}, T_n)$  by restricting  $\psi_j^{\omega^+}(x, t)$  onto  $\omega \times (T_{n-1}, T_n)$ . Finally, the offline basis functions on  $\omega \times (T_{n-1}, T_n)$  are defined by  $\phi_j^\omega(x, t) = \chi \psi_j^\omega(x, t)$ , where  $\chi$  is the standard multiscale basis function from (9) for a generic coarse neighborhood  $\omega$ . We also define the local offline space on  $\omega \times (T_{n-1}, T_n)$  as

$$V_{\text{off}}^\omega = \text{span}\{\phi_j^\omega(x, t) | j = 1, \dots, L^\omega\}.$$

Note that one can take  $V_H^{(n)}$  in (5) as  $V_H^{(n)} = V_{\text{off}}^{(n)} = \text{span}\{\phi_j^{\omega_i}(x, t) | 1 \leq i \leq N_c, 1 \leq j \leq L_i\}$ . As a result,  $V_H = V_{\text{off}} = \bigoplus_{n=1}^N V_H^{(n)}$ .

**Remark 2.1.** For the convenience of convergence analysis in Section 3, we also denote by  $\{\Psi_1^{\omega^+, \text{off}}, \dots, \Psi_{L^\omega + p_{\text{bf}}^\omega}^{\omega^+, \text{off}}\}$  all the eigenfunctions from (7) corresponding to the ordered eigenvalues, and define

$$\psi_j^{\omega^+}(x, t) = \sum_{k=1}^{L^\omega + p_{\text{bf}}^\omega} (\Psi_j^{\omega^+, \text{off}})_k \psi_k^+(x, t), \quad j = 1, 2, \dots, L^\omega + p_{\text{bf}}^\omega.$$

We note that the snapshot space on  $\omega^+ \times (T_{n-1}^*, T_n)$  can be rewritten as

$$V_{\text{snap}}^{\omega^+} = \text{span}\{\psi_j^{\omega^+}(x, t) | j = 1, \dots, L^\omega + p_{\text{bf}}^\omega\},$$

and the snapshot space on  $\omega \times (T_{n-1}, T_n)$  can be written as

$$V_{\text{snap}}^\omega = \text{span}\{\psi_j^\omega(x, t) | j = 1, \dots, L^\omega + p_{\text{bf}}^\omega\},$$

where each  $\psi_j^\omega(x, t)$  is the restriction of  $\psi_j^{\omega^+}(x, t)$  onto  $\omega \times (T_{n-1}, T_n)$ . By collecting all local snapshot spaces on each  $\omega \times (T_{n-1}, T_n)$ , we can obtain the snapshot space  $V_{\text{snap}}^{(n)}$  on  $\Omega \times (T_{n-1}, T_n)$ .

The offline space can be rewritten as

$$V_{\text{off}}^\omega = \text{span}\{\chi \psi_j^\omega(x, t) | j \leq L^\omega\}.$$

**Remark 2.2.** One can use a more general spectral problem in (7) with

$$\begin{aligned} A(\phi, v) &= \frac{1}{2} \left( \int_\omega \phi(x, T_n) v(x, T_n) + \int_\omega \phi(x, T_{n-1}) v(x, T_{n-1}) \right) + \int_{T_{n-1}}^{T_n} \int_\omega \kappa(x, t) \nabla \phi \cdot \nabla v \\ &\quad + \int_{T_{n-1}}^{T_n} \int_\omega \kappa(x, t) (z_\phi z_v + \nabla z_\phi \cdot \nabla z_v), \\ S(\phi, v) &= \int_\omega \phi(x, T_{n-1}) v(x, T_{n-1}) + \int_{T_{n-1}}^{T_n} \int_\omega \tilde{\kappa}(x, t) \phi v + \int_{T_{n-1}}^{T_n} \int_\omega \kappa |\nabla \chi|^2 z_\phi z_v, \end{aligned} \tag{10}$$

where for any  $w \in V_{\text{snap}}^\omega$ ,  $z_w$  satisfies

$$-z_w(x, t) + \nabla \cdot (\kappa(x, t) \nabla z_w(x, t)) = \chi \frac{\partial w}{\partial t}, \quad \forall t \in (T_{n-1}, T_n).$$

With this spectral problem, one can simplify the proof presented in Section 3. However, the numerical implementation of this local spectral problem is more complicated.

### 3 Convergence analysis

In this section, we will analyze the convergence of our proposed method. To start, we firstly define two norms that are used in the analysis. We define  $\|\cdot\|_{V^{(n)}}^2$  and  $\|\cdot\|_{W^{(n)}}^2$  by

$$\begin{aligned}\|u\|_{V^{(n)}}^2 &= \int_{T_{n-1}}^{T_n} \int_{\Omega} \kappa |\nabla u|^2 + \frac{1}{2} \int_{\Omega} u^2(x, T_n^-) + \frac{1}{2} \int_{\Omega} u^2(x, T_{n-1}^+), \\ \|u\|_{W^{(n)}}^2 &= \|u\|_{V^{(n)}}^2 + \int_{T_{n-1}}^{T_n} \|u_t(\cdot, t)\|_{H^{-1}(\kappa, \Omega)}^2,\end{aligned}$$

where

$$\|u\|_{H^{-1}(\kappa, \Omega)} = \sup_{v \in H_0^1(\Omega)} \frac{\int_{\Omega} uv}{(\int_{\Omega} \kappa |\nabla v|^2)^{\frac{1}{2}}}.$$

In the following, we will show the  $V^{(n)}$ -norm of the error  $u_h - u_H$  can be bounded by the  $W^{(n)}$ -norm of the difference  $u_h - w$  for any  $w \in V_H^{(n)}$ , where  $u_h$  is the fine scale solution from Eqn.(3),  $u_H$  is the multiscale solution from Eqn.(5), and  $V_H^{(n)}$  is the multiscale space defined in the previous section. The proof of this lemma will be presented in the Appendix.

**Lemma 3.1.** *Let  $u_h$  be the fine scale solution from Equation (3),  $u_H$  be the multiscale solution from Equation (5). We have the following estimate*

$$\|u_h - u_H\|_{V^{(n)}}^2 \leq \begin{cases} C \|u_h - w\|_{W^{(n)}}^2 & \text{for } n = 1, \\ C (\|u_h - w\|_{W^{(n)}}^2 + \|u_h - u_H\|_{V^{(n-1)}}^2) & \text{for } n > 1, \end{cases}$$

for any  $w \in V_H^{(n)}$ . If we define the  $V^{(0)}$ -norm to be 0, then we can write

$$\|u_h - u_H\|_{V^{(n)}}^2 \leq C (\|u_h - w\|_{W^{(n)}}^2 + \|u_h - u_H\|_{V^{(n-1)}}^2) \quad \text{for } n \geq 1,$$

for any  $w \in V_H^{(n)}$ .

Therefore, to estimate the error of our multiscale solution, we only need to find a function  $w$  in  $V_H^{(n)}$  such that  $\|u_h - w\|_{W^{(n)}}$  is small. Except for Lemma 3.1, we still need the following lemma to estimate  $\|u_h - w\|_{W^{(n)}}$ .

**Lemma 3.2.** *For any  $v$  satisfying*

$$\frac{\partial}{\partial t} v - \operatorname{div}(\kappa(x, t) \nabla v) = 0 \quad \text{in } \omega_i \times (T_{n-1}, T_n),$$

we have

$$\int_{\omega_i} \chi_i^2 v^2(x, T_n) + \int_{T_{n-1}}^{T_n} \int_{\omega_i} \kappa |\chi_i^2 \nabla v|^2 \preceq \int_{\omega_i} \chi_i^2 v^2(x, T_{n-1}) + \int_{T_{n-1}}^{T_n} \int_{\omega_i} \kappa |\nabla \chi_i|^2 v^2, \quad (11)$$

where the notation  $F \preceq G$  means  $F \leq CG$  with a constant  $C$  independent of the mesh, contrast and the functions involved.

Now, we are ready to prove our main result in this section.

**Theorem 3.3.** *Let  $u_h$  be the fine scale solution from Equation (3),  $u_H$  be the multiscale solution from Equation (5). Let  $\tilde{u}_h = \operatorname{argmin}_{v \in V_{snap}^{(n)}} \{\|u_h - v\|_{W^{(n)}}\}$  and we denote  $\tilde{u}_h = \sum_i \chi_i \tilde{u}_{h,i}$  with  $\tilde{u}_{h,i} = \sum_j c_{i,j} \psi_j^{\omega_i}$ . There holds*

$$\|u_h - u_H\|_{V^{(n)}}^2 \preceq M(DEF + 1) \sum_i \left( \frac{1}{\lambda_{L_i+1}^{\omega_i^+}} \|\tilde{u}_{h,i}^+\|_{V^{(n)}(\omega_i^+)}^2 \right) + \|u_h - \tilde{u}_h\|_{W^{(n)}}^2 + \|u_h - u_H\|_{V^{(n-1)}}^2,$$



where

$M = \max_K \{M_K\}$  with  $M_K$  is the number of coarse neighborhoods  $\omega_i$ 's which have nonempty intersection with  $K$ ,

$$D = \max\{D_i\} \text{ with } D_i = \sup_{v \in H_0^1(\Omega)} \frac{\int_{\omega_i} \kappa |\nabla \chi_i|^2 v^2 + \int_{\omega_i} \kappa \chi_i^2 |\nabla v|^2}{\int_{\omega_i} \kappa |\nabla v|^2 + \int_{\omega_i} \kappa v^2},$$

$$E = \sup_{w \in H_0^1(\Omega)} \frac{\int_{\Omega} \kappa |\nabla w|^2 + \int_{\Omega} \kappa w^2}{\int_{\Omega} \kappa |\nabla w|^2},$$

$$F = \max\{F_i\} \text{ with } F_i = \frac{1}{\min_{x \in \omega_i} \{|\chi_i^+(x)|^2\}},$$

$\tilde{u}_{h,i}^+ = \sum_j c_{i,j} \psi_j^{\omega_i^+}$  and the local norm  $\|\cdot\|_{V^{(n)}(\omega_i^+)}$  is defined by

$$\|v\|_{V^{(n)}(\omega_i^+)}^2 = \int_{T_{n-1}}^{T_n} \int_{\omega_i^+} \kappa |\nabla v|^2 + \frac{1}{2} \int_{\omega_i^+} v^2(x, T_n^-) + \frac{1}{2} \int_{\omega_i^+} v^2(x, T_{n-1}^+).$$

*Proof.* By Lemma 3.1,

$$\|u_h - u_H\|_{V^{(n)}}^2 \leq \inf_{w \in V_H^{(n)}} \|u_h - w\|_{W^{(n)}}^2 + \|u_h - u_H\|_{V^{(n-1)}}^2. \quad (12)$$

Therefore, we need to estimate  $\inf_{w \in V_H^{(n)}} \|u_h - w\|_{W^{(n)}}$ . Note that  $\tilde{u}_h = \sum_i \chi_i \tilde{u}_{h,i} = \sum_i \sum_j c_{i,j} \chi_i \psi_j^{\omega_i}$ . Using this expression, we can define a projection of  $\tilde{u}_h$  into  $V_H^{(n)}$  by

$$P(\tilde{u}_h) = \sum_i \sum_{j \leq L_i} c_{i,j} \chi_i \psi_j^{\omega_i}.$$

Then

$$\begin{aligned} \inf_{w \in V_H^{(n)}} \|u_h - w\|_{W^{(n)}}^2 &\leq \|u_h - P(\tilde{u}_h)\|_{W^{(n)}}^2 \\ &\leq \|u_h - \tilde{u}_h\|_{W^{(n)}}^2 + \|\tilde{u}_h - P(\tilde{u}_h)\|_{W^{(n)}}^2. \end{aligned} \quad (13)$$

We will estimate  $\|\tilde{u}_h - P(\tilde{u}_h)\|_{W^{(n)}}$ .

By the definition of  $\|\cdot\|_{W^{(n)}}$ , we have

$$\|\tilde{u}_h - P(\tilde{u}_h)\|_{W^{(n)}}^2 = \left\| \sum_i \chi_i (\tilde{u}_{h,i} - P(\tilde{u}_{h,i})) \right\|_{V^{(n)}}^2 + \int_{T_{n-1}}^{T_n} \left\| \frac{\partial(\sum_i \chi_i (\tilde{u}_{h,i} - P(\tilde{u}_{h,i})))}{\partial t} \right\|_{H^{-1}(\kappa, \Omega)}^2,$$

where  $\tilde{u}_{h,i} = \sum_j c_{i,j} \psi_j^{\omega_i}$  and  $P(\tilde{u}_{h,i}) = \sum_{j \leq L_i} c_{i,j} \psi_j^{\omega_i}$ . Let  $e_i = \tilde{u}_{h,i} - P(\tilde{u}_{h,i})$ , then  $\tilde{u}_h - P(\tilde{u}_h) = \sum_i \chi_i e_i$ . Therefore,

$$\|\tilde{u}_h - P(\tilde{u}_h)\|_{W^{(n)}}^2 = \left\| \sum_i \chi_i e_i \right\|_{V^{(n)}}^2 + \int_{T_{n-1}}^{T_n} \left\| \frac{\partial(\sum_i \chi_i e_i)}{\partial t} \right\|_{H^{-1}(\kappa, \Omega)}^2. \quad (14)$$

In the following, we will estimate the two terms on the right hand side of (14), separately. Then the proof is done.

First, we estimate the term  $\|\sum_i \chi_i e_i\|_{V^{(n)}}$ . We define the local norm  $\|\cdot\|_{V^{(n)}(K)}$  by

$$\|v\|_{V^{(n)}(K)}^2 = \int_{T_{n-1}}^{T_n} \int_K \kappa |\nabla v|^2 + \frac{1}{2} \int_K v^2(x, T_n^-) + \frac{1}{2} \int_K v^2(x, T_{n-1}^+).$$

Then we have

$$\left\| \sum_i \chi_i e_i \right\|_{V^{(n)}}^2 \leq \sum_K \left\| \sum_i \chi_i e_i \right\|_{V^{(n)}(K)}^2.$$

Moreover,

$$\left\| \sum_i \chi_i e_i \right\|_{V^{(n)}(K)}^2 \leq M_K \sum_i \|\chi_i e_i\|_{V^{(n)}(K)}^2,$$

where  $M_K$  is the number of coarse neighborhoods  $\omega_i$ 's which have nonempty intersection with  $K$ . Therefore,

$$\begin{aligned} \left\| \sum_i \chi_i e_i \right\|_{V^{(n)}}^2 &\leq \sum_K M_K \sum_i \|\chi_i e_i\|_{V^{(n)}(K)}^2 \\ &\leq M \sum_i \|\chi_i e_i\|_{V^{(n)}(\omega_i)}^2, \end{aligned} \quad (15)$$

where  $M = \max_K \{M_K\}$ . Now, we need to estimate the term  $\|\chi_i e_i\|_{V^{(n)}(\omega_i)}^2$ . Since  $\nabla(\chi_i e_i) = e_i \nabla \chi_i + \chi_i \nabla e_i$ , we obtain

$$\begin{aligned} \|\chi_i e_i\|_{V^{(n)}(\omega_i)}^2 &\leq 2 \int_{T_{n-1}}^{T_n} \int_{\omega_i} \kappa |\nabla \chi_i|^2 e_i^2 + 2 \int_{T_{n-1}}^{T_n} \int_{\omega_i} \kappa \chi_i^2 |\nabla e_i|^2 \\ &\quad + \frac{1}{2} \int_{\omega_i} \chi_i^2 e_i^2(x, T_n^-) + \frac{1}{2} \int_{\omega_i} \chi_i^2 e_i^2(x, T_{n-1}^+). \end{aligned}$$

Using Lemma 3.2, we have

$$\begin{aligned} \|\chi_i e_i\|_{V^{(n)}(\omega_i)}^2 &\leq \int_{T_{n-1}}^{T_n} \int_{\omega_i} \kappa |\nabla \chi_i|^2 e_i^2 + \int_{\omega_i} \chi_i^2 e_i^2(x, T_{n-1}^+) \\ &\leq \int_{T_{n-1}}^{T_n} \int_{\omega_i} \kappa |\nabla \chi_i|^2 e_i^2 + \int_{\omega_i} e_i^2(x, T_{n-1}^+). \end{aligned}$$

Now we introduce notations in  $\omega_i^+$  and denote  $e_i^+ = \tilde{u}_{h,i}^+ - P(\tilde{u}_{h,i}^+)$ , where  $\tilde{u}_{h,i}^+ = \sum_j c_{i,j} \psi_j^{\omega_i^+}$  and  $P(\tilde{u}_{h,i}^+) = \sum_{j \leq L_i} c_{i,j} \psi_j^{\omega_i^+}$ . It is obvious that  $\tilde{u}_{h,i}^+|_{\omega_i} = \tilde{u}_{h,i}$ ,  $P(\tilde{u}_{h,i}^+)|_{\omega_i} = P(\tilde{u}_{h,i})$  and  $e_i^+|_{\omega_i} = e_i$ . And there holds the following two inequalities,

$$\int_{T_{n-1}}^{T_n} \int_{\omega_i} \kappa |\nabla \chi_i|^2 e_i^2 \leq \int_{T_{n-1}}^{T_n} \int_{\omega_i^+} \kappa |\nabla \chi_i^+|^2 |e_i^+|^2, \quad (16)$$

and

$$\int_{\omega_i} e_i^2(x, T_{n-1}^+) \leq \int_{\omega_i^+} |e_i^+(x, T_{n-1}^+)|^2. \quad (17)$$

Thus,

$$\|\chi_i e_i\|_{V^{(n)}(\omega_i)}^2 \leq \int_{T_{n-1}}^{T_n} \int_{\omega_i^+} \kappa |\nabla \chi_i^+|^2 |e_i^+|^2 + \int_{\omega_i^+} |e_i^+(x, T_{n-1}^+)|^2. \quad (18)$$

Substituting (18) into (15), we immediately obtain

$$\left\| \sum_i \chi_i e_i \right\|_{V^{(n)}}^2 \leq M \sum_i \left( \int_{T_{n-1}}^{T_n} \int_{\omega_i^+} \kappa |\nabla \chi_i^+|^2 |e_i^+|^2 + \int_{\omega_i^+} |e_i^+(x, T_{n-1}^+)|^2 \right). \quad (19)$$

Next, we will estimate the term  $\int_{T_{n-1}}^{T_n} \left\| \frac{\partial(\sum_i \chi_i e_i)}{\partial t} \right\|_{H^{-1}(\kappa, \Omega)}^2$ . By definition, we have

$$\begin{aligned} \int_{T_{n-1}}^{T_n} \left\| \frac{\partial(\sum_i \chi_i e_i)}{\partial t} \right\|_{H^{-1}(\kappa, \Omega)}^2 &= \int_{T_{n-1}}^{T_n} \sup_{w \in H_0^1(\Omega)} \frac{(\int_{\Omega} \sum_i \chi_i \frac{\partial e_i}{\partial t} w)^2}{\int_{\Omega} \kappa |\nabla w|^2} \\ &\leq \int_{T_{n-1}}^{T_n} \sup_{w \in H_0^1(\Omega)} \frac{(\sum_i |\int_{\omega_i} \chi_i \frac{\partial e_i}{\partial t} w|)^2}{\int_{\Omega} \kappa |\nabla w|^2}. \end{aligned} \quad (20)$$

Since  $e_i$  satisfies the equation

$$\frac{\partial}{\partial t} e_i - \operatorname{div}(\kappa(x, t) \nabla e_i) = 0 \text{ in } \omega_i \times (T_{n-1}, T_n),$$

we have

$$\begin{aligned} \int_{\omega_i} \chi_i \frac{\partial e_i}{\partial t} w &= - \int_{\omega_i} \kappa(x, t) \nabla e_i \cdot \nabla(\chi_i w) \\ &= - \int_{\omega_i} \kappa(x, t) w \nabla e_i \cdot \nabla \chi_i - \int_{\omega_i} \kappa(x, t) \chi_i \nabla e_i \cdot \nabla w. \end{aligned}$$

Moreover,

$$\begin{aligned} \left| \int_{\omega_i} \chi_i \frac{\partial e_i}{\partial t} w \right| &= \left| - \int_{\omega_i} \kappa w \nabla e_i \cdot \nabla \chi_i - \int_{\omega_i} \kappa \chi_i \nabla e_i \cdot \nabla w \right| \\ &\leq \left( \int_{\omega_i} \kappa w^2 |\nabla \chi_i|^2 \right)^{\frac{1}{2}} \left( \int_{\omega_i} \kappa |\nabla e_i|^2 \right)^{\frac{1}{2}} + \left( \int_{\omega_i} \kappa \chi_i^2 |\nabla w|^2 \right)^{\frac{1}{2}} \left( \int_{\omega_i} \kappa |\nabla e_i|^2 \right)^{\frac{1}{2}} \\ &\leq 2 \left( \int_{\omega_i} \kappa w^2 |\nabla \chi_i|^2 + \int_{\omega_i} \kappa \chi_i^2 |\nabla w|^2 \right)^{\frac{1}{2}} \left( \int_{\omega_i} \kappa |\nabla e_i|^2 \right)^{\frac{1}{2}}. \end{aligned} \quad (21)$$

Let

$$D_i = \sup_{v \in H_0^1(\Omega)} \frac{\int_{\omega_i} \kappa |\nabla \chi_i|^2 v^2 + \int_{\omega_i} \kappa \chi_i^2 |\nabla v|^2}{\int_{\omega_i} \kappa |\nabla v|^2 + \int_{\omega_i} \kappa v^2}.$$

From (21), we obtain

$$\left| \int_{\omega_i} \chi_i \frac{\partial e_i}{\partial t} w \right| \leq 2D_i^{\frac{1}{2}} \left( \int_{\omega_i} \kappa |\nabla w|^2 + \int_{\omega_i} \kappa w^2 \right)^{\frac{1}{2}} \left( \int_{\omega_i} \kappa |\nabla e_i|^2 \right)^{\frac{1}{2}}.$$

Therefore,

$$\begin{aligned} \sum_i \left| \int_{\omega_i} \chi_i \frac{\partial e_i}{\partial t} w \right| &\leq 2 \sum_i D_i^{\frac{1}{2}} \left( \int_{\omega_i} \kappa |\nabla w|^2 + \int_{\omega_i} \kappa w^2 \right)^{\frac{1}{2}} \left( \int_{\omega_i} \kappa |\nabla e_i|^2 \right)^{\frac{1}{2}} \\ &\leq 2 \left( \sum_i D_i \left( \int_{\omega_i} \kappa |\nabla w|^2 + \int_{\omega_i} \kappa w^2 \right) \right)^{\frac{1}{2}} \left( \sum_i \int_{\omega_i} \kappa |\nabla e_i|^2 \right)^{\frac{1}{2}} \\ &\leq 2D^{\frac{1}{2}} M^{\frac{1}{2}} \left( \int_{\Omega} \kappa |\nabla w|^2 + \int_{\Omega} \kappa w^2 \right)^{\frac{1}{2}} \left( \sum_i \int_{\omega_i} \kappa |\nabla e_i|^2 \right)^{\frac{1}{2}}, \end{aligned} \quad (22)$$

where  $D = \max\{D_i\}$ . Combining (20) with (22), we have

$$\int_{T_{n-1}}^{T_n} \left\| \frac{\partial(\sum_i \chi_i e_i)}{\partial t} \right\|_{H^{-1}(\kappa, \Omega)}^2 \leq 4DM \sup_{w \in H^1(\Omega)} \frac{(\int_{\Omega} \kappa |\nabla w|^2 + \int_{\Omega} \kappa w^2)}{\int_{\Omega} \kappa |\nabla w|^2} \left( \sum_i \int_{T_{n-1}}^{T_n} \int_{\omega_i} \kappa |\nabla e_i|^2 \right).$$

Let

$$E = \sup_{w \in H_0^1(\Omega)} \frac{\int_{\Omega} \kappa |\nabla w|^2 + \int_{\Omega} \kappa w^2}{\int_{\Omega} \kappa |\nabla w|^2},$$

then we have

$$\int_{T_{n-1}}^{T_n} \left\| \frac{\partial(\sum_i \chi_i e_i)}{\partial t} \right\|_{H^{-1}(\kappa, \Omega)}^2 \leq 4DME \left( \sum_i \int_{T_{n-1}}^{T_n} \int_{\omega_i} \kappa |\nabla e_i|^2 \right). \quad (23)$$

Now, we substitute (23) and (19) into (14), then we have

$$\begin{aligned} \|\tilde{u}_h - P(\tilde{u}_h)\|_{W(n)}^2 &\leq M \sum_i \left( DE \int_{T_{n-1}}^{T_n} \int_{\omega_i} \kappa |\nabla e_i|^2 + \int_{T_{n-1}}^{T_n} \int_{\omega_i} \kappa |\nabla \chi_i|^2 e_i^2 + \int_{\omega_i} \chi_i^2 e_i^2(x, T_{n-1}^+) \right) \\ &\leq M \sum_i \left( DE \int_{T_{n-1}}^{T_n} \int_{\omega_i} \kappa |\nabla e_i|^2 + \int_{T_{n-1}}^{T_n} \int_{\omega_i} \kappa |\nabla \chi_i|^2 e_i^2 + \int_{\omega_i} e_i^2(x, T_{n-1}^+) \right). \end{aligned} \quad (24)$$

Note that

$$\begin{aligned} \int_{T_{n-1}}^{T_n} \int_{\omega_i} \kappa |\nabla e_i|^2 &\leq \int_{T_{n-1}}^{T_n} \frac{1}{\min_{x \in \omega_i} \{|\chi_i^+(x)|^2\}} \int_{\omega_i} \kappa |\chi_i^+|^2 |\nabla e_i|^2 \\ &\leq \frac{1}{\min_{x \in \omega_i} \{|\chi_i^+(x)|^2\}} \int_{T_{n-1}}^{T_n} \int_{\omega_i^+} \kappa |\chi_i^+|^2 |\nabla e_i^+|^2. \end{aligned}$$

Applying Lemma 3.2 for  $\omega_i^+$  then implies

$$\begin{aligned} \int_{T_{n-1}}^{T_n} \int_{\omega_i} \kappa |\nabla e_i|^2 &\leq \frac{1}{\min_{x \in \omega_i} \{|\chi_i^+(x)|^2\}} \left( \int_{T_{n-1}}^{T_n} \int_{\omega_i^+} \kappa |\nabla \chi_i^+|^2 |e_i^+|^2 + \int_{\omega_i^+} |\chi_i^+|^2 |e_i^+(x, T_{n-1}^+)|^2 \right) \\ &\leq F_i \left( \int_{T_{n-1}}^{T_n} \int_{\omega_i^+} \kappa |\nabla \chi_i^+|^2 |e_i^+|^2 + \int_{\omega_i^+} |e_i^+(x, T_{n-1}^+)|^2 \right), \end{aligned} \quad (25)$$

where  $F_i = \frac{1}{\min_{x \in \omega_i} \{|\chi_i^+(x)|^2\}}$ . Substituting (25), (16) and (17) into (24) gives

$$\begin{aligned} \|\tilde{u}_h - P(\tilde{u}_h)\|_{W(n)}^2 &\leq M \sum_i (DEF_i + 1) \left( \int_{T_{n-1}}^{T_n} \int_{\omega_i^+} \kappa |\nabla \chi_i^+|^2 |e_i^+|^2 + \int_{\omega_i^+} |e_i^+(x, T_{n-1}^+)|^2 \right) \\ &\leq M(DEF + 1) \sum_i \left( \int_{T_{n-1}}^{T_n} \int_{\omega_i^+} \tilde{\kappa}^+(x, t) |e_i^+|^2 + \int_{\omega_i^+} |e_i^+(x, T_{n-1}^+)|^2 \right), \end{aligned} \quad (26)$$

where  $F = \max\{F_i\}$ . Using the spectral problem, we have

$$\|\tilde{u}_h - P(\tilde{u}_h)\|_{W(n)}^2 \leq M(DEF + 1) \sum_i \left( \frac{1}{\lambda_{L_i+1}^{\omega_i^+}} \|\tilde{u}_{h,i}^+\|_{V(n)(\omega_i^+)}^2 \right). \quad (27)$$

Combine (12), (13) and (27), and we finally obtain

$$\|u_h - u_H\|_{V(n)}^2 \leq M(DEF + 1) \sum_i \left( \frac{1}{\lambda_{L_i+1}^{\omega_i^+}} \|\tilde{u}_{h,i}^+\|_{V(n)(\omega_i^+)}^2 \right) + \|u_h - \tilde{u}_h\|_{W(n)}^2 + \|u_h - u_H\|_{V(n-1)}^2.$$

□

## 4 Numerical results. Offline GMsFEM.

In this section, we present a number of representative numerical examples to show the performance of the proposed method. In particular, we solve Equation (2) using the space-time GMsFEM to validate the effectiveness of the proposed approaches. The space domain  $\Omega$  is taken as the unit square  $[0, 1] \times [0, 1]$  and is divided into  $10 \times 10$  coarse blocks consisting of uniform squares. Each coarse block is then divided into  $10 \times 10$  fine blocks consisting of uniform squares. That is,  $\Omega$  is partitioned by  $100 \times 100$  square fine-grid blocks. The whole time interval is  $[0, 1.6]$  (i.e.,  $T = 1.6$ ) and is divided into two uniform coarse time intervals and each coarse time interval is then divided into 8 fine time intervals. We also use a source term  $f = 1$  and impose a continuous initial condition  $\beta(x, y) = \sin(\pi x) \sin(\pi y)$ . We employ three different high-contrast permeability fields  $\kappa(x, t)$ 's to examine our method, which will be shown in the following three cases separately. In each case, we first solve for  $u_h$  from Equation (3) to obtain the fine-grid solution. Then we solve for the multiscale solution  $u_H$  using the space-time GMsFEM. To compare the accuracy, we will use the following error quantities:

$$e_1 = \left( \frac{\int_0^T \|u_H(t) - u_h(t)\|_{L^2(\Omega)}^2}{\int_0^T \|u_h(t)\|_{L^2(\Omega)}^2} \right)^{1/2}, \quad e_2 = \left( \frac{\int_0^T \int_{\Omega} \kappa |\nabla(u_H(t) - u_h(t))|^2}{\int_0^T \int_{\Omega} \kappa |\nabla u_h(t)|^2} \right)^{1/2}. \quad (28)$$

Since we are using the technique of randomized oversampling in the computation of the snapshot space, we would like to introduce the concept of *snapshot ratio*, which is calculated as the number of randomized snapshots divided by the number of the full snapshots on one coarse neighborhood  $\omega_i$ . Here, the number of the full snapshots refers to the number of functions  $\delta_i(x, t)$  from Equation (6). In the following experiment with  $100 \times 100$  fine-grid mesh, this number of the full snapshots on each coarse neighborhood is calculated by  $n_{\text{total}}^{\text{snap}} = 21 \times 21 + 40 \times 8 = 761$ .

### 4.1 High-contrast Permeability Field 1: High-contrast medium translated in time

We start with a high-contrast permeability field  $\kappa(x, t)$ , which is translated uniformly after every other fine time step. High-contrast permeability fields at the initial and final time steps are shown in Figure 2. Next, we consider applying the space-time GMsFEM to Equation (2) and solve for the multiscale solution  $u_H$ . Recall the procedures that are described in the Section 2, where we need to construct the snapshot spaces in the first place. The number of local offline basis that will be used in each  $\omega_i$ , denoted by  $L_i$ , and the buffer number  $p_{\text{bf}}$  needs to be chosen in advance since they determine how many local snapshots are used. Then we can construct the lower dimensional offline space by performing space reduction on the snapshot space. In our experiments, we use the same buffer number and the same number of local offline basis for all coarse neighborhood  $\omega_i$ 's.

First, we fix  $L_i = 11$  for all  $\omega_i$ 's and examine the influences of various buffer numbers on the solution errors  $e_1$  and  $e_2$ . The results are displayed in the left table of Table 1. It is observed that when increasing the buffer numbers, one can get more accurate solutions, which is as expected. But the error decays very slowly, which indicates that using different buffer numbers doesn't affect the convergence rate too much. Based on this observation, it is not necessary to choose a large buffer number in order to improve convergence rate. Then we consider the choice of  $L_i$ , the number of eigenbasis in a neighborhood. With the fixed buffer number  $p_{\text{bf}} = 8$ , we examine the convergence behaviors of using different  $L_i$ 's. Relative errors of multiscale solutions are shown in the right table of Table 1. We observe that with a fixed buffer number, the relative errors are decreasing as using more offline basis. To see a more quantitative relationship between the relative errors and the values of  $L_i$  as well as being inspired by the result in Theorem 3.3, we inspect the values of  $1/\Lambda_*$  and the corresponding squared errors (see Table 2 and Figure 3), where  $\Lambda_* = \min_{\omega_i} \lambda_{L_i+1}^{\omega_i}$  and  $\{\lambda_j^{\omega_i}\}$  are the eigenvalues associated with the eigenbasis computed by spectral problem (7) in each  $\omega_i$ . We note that when plotting Figure 3, we don't use the values of case  $L_i = 2$ , because in this case as in the case with one basis function per node, the method does not converge as we do not have sufficient number of basis functions. We

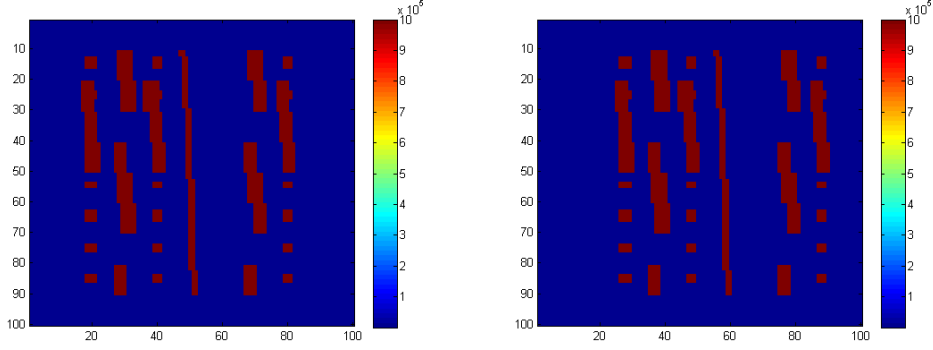


Figure 2: High-contrast Permeability Field 1. Left: the permeability at the initial time. Right: the permeability at the final time.

note that the two curves in Figure 3 track each other somewhat closely. This indicates that  $1/\Lambda_*$ 's and  $e_2^2$ 's are correlated and we calculate for the correlation coefficient to be  $corrcoef(1/\Lambda_*, e_2^2) = 0.9778$ .

Observing the dimensions of the offline spaces  $V_{\text{off}}$ , one can see that compared with the traditional fine-scale finite element method, the proposed space-time GMsFEM uses much fewer degrees of freedom while achieving an accurate solution. Also, by inspecting the snapshot ratios, one can see that the use of randomization can reduce the dimension of snapshot spaces substantially. We would like to comment that oversampling technique is necessary for the randomization. For example, in the case  $L_i = 6$  and  $p_{\text{bf}} = 8$ , if without oversampling the errors  $e_1$  and  $e_2$  are 11.19% and 88.42%, respectively, which are worse than the errors obtained with oversampling.

$p_{\text{bf}}$	Snapshot ratio	$e_1$	$e_2$	$L_i$	$\dim(V_{\text{off}})$	Snapshot ratio	$e_1$	$e_2$
1	0.0158	6.18%	53.90%	2	162	0.0131	17.03%	129.14%
4	0.0197	5.66%	48.04%	6	486	0.0184	8.11%	62.59%
8	0.0250	5.17%	45.86%	10	810	0.0237	6.97%	54.85%
12	0.0302	5.16%	43.83%	20	1620	0.0368	4.81%	41.18%
20	0.0407	4.71%	41.14%	30	2430	0.0499	3.29%	31.64%
30	0.0539	4.35%	38.68%	40	3240	0.0631	2.28%	24.43%
40	0.0670	4.23%	37.60%	50	4050	0.0762	1.54%	18.45%

Table 1: First permeability field. Left: errors with the fixed number of offline basis  $L_i = 11$ . Right: errors with the fixed buffer number  $p_{\text{bf}} = 8$ .

$L_i$	$1/\Lambda_*$	$e_1^2$	$e_2^2$
2	0.2734	2.90%	166.78%
6	0.0120	0.66%	39.17%
10	0.0085	0.49%	30.08%
20	0.0061	0.23%	16.96%
30	0.0053	0.11%	10.01%
40	0.0048	0.05%	5.97%
50	0.0042	0.02%	3.40%

Table 2:  $1/\Lambda_*$  values and errors.

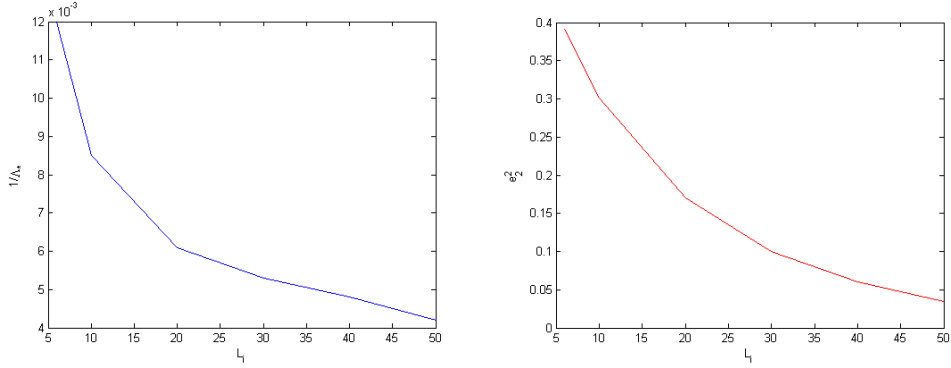


Figure 3: Left:  $1/\Lambda_*$  vs  $L_i$ ; Right:  $e_2^2$  vs  $L_i$ .

## 4.2 High-contrast Permeability Field 2: Four channels translated in time

In this subsection, we consider a more structured high-contrast permeability field  $\kappa(x, t)$ , which has four channels inside and these four channels are translated uniformly in time. High-contrast permeability fields at the initial and final time steps are shown in Figure 4. We repeat our steps from the previous example by fixing  $L_i$  and  $p_{\text{bf}}$ , separately. The results are shown in Table 3. One can still observe that increasing the buffer numbers will slowly reduce the relative errors and with a fixed buffer number, the relative errors are decreasing as adding more offline basis. Using a similar approach, we can also get the cross-correlation coefficient between  $e_2^2$  and  $1/\Lambda_*$ , which is 0.9863. This suggests a linear relationship between  $e_2^2$  and  $1/\Lambda_*$  and verifies Theorem 3.3.

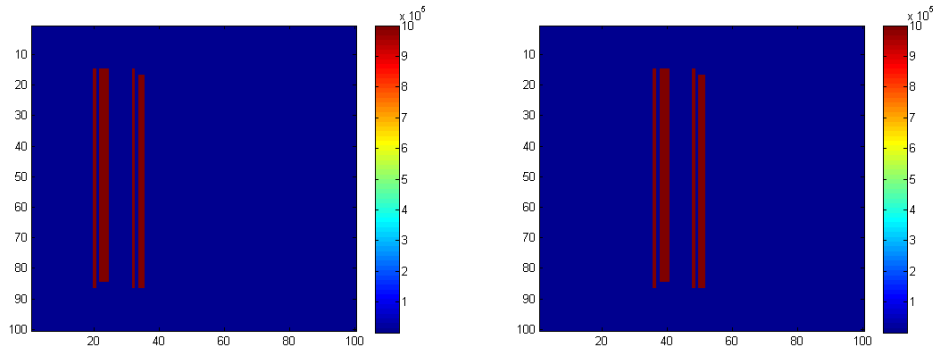


Figure 4: High-contrast Permeability Field 2. Left: the permeability at the initial time. Right: the permeability at the final time.

$p_{\text{bf}}$	Snapshot ratio	$e_1$	$e_2$	$L_i$	$\dim(V_{\text{off}})$	Snapshot ratio	$e_1$	$e_2$
1	0.0158	7.42%	61.87%	2	162	0.0131	11.91%	104.95%
4	0.0197	7.30%	58.95%	6	486	0.0184	8.33%	70.82%
8	0.0250	7.14%	57.30%	10	810	0.0237	7.25%	58.25%
12	0.0302	7.00%	54.01%	20	1620	0.0368	5.67%	43.10%
20	0.0407	6.81%	50.85%	30	2430	0.0499	3.90%	32.75%
30	0.0539	6.61%	49.30%	40	3240	0.0631	2.73%	27.08%
40	0.0670	6.43%	48.26%	50	4050	0.0762	1.86%	20.70%

Table 3: Second permeability field. Left: errors with the fixed number of offline basis  $L_i = 11$ . Right: errors with the fixed buffer number  $p_{\text{bf}} = 8$ .

### 4.3 High-contrast Permeability Field 3: Four channels rotated in time

In the third example, we consider another structured high-contrast permeability field  $\kappa(x, t)$  which has four channels inside and these four channels are rotated anticlockwise around the center by 11.25 degrees after each fine time step. High contrast permeability fields at the initial time step is shown in Figure 5. We repeat the same procedures as in the previous two examples. The results are shown in Table 4 and one can draw similar conclusions as before. The cross-correlation coefficient between  $e_2^2$  and  $1/\Lambda_*$  is calculated as 0.9959. This shows a linear relationship between  $e_2^2$  and  $1/\Lambda_*$  (see Theorem 3.3).

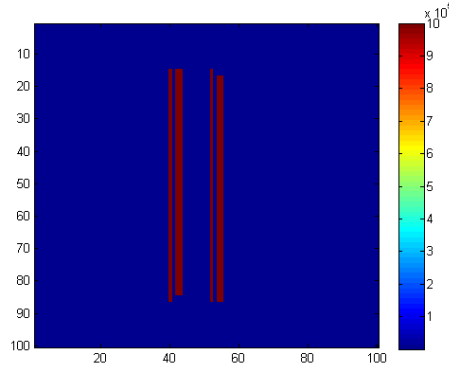


Figure 5: High-contrast Permeability Field 3 at the initial time.

$p_{\text{bf}}$	Snapshot ratio	$e_1$	$e_2$	$L_i$	$\dim(V_{\text{off}})$	Snapshot ratio	$e_1$	$e_2$
1	0.0158	8.68%	72.86%	2	162	0.0131	10.41%	109.40%
4	0.0197	8.67%	71.67%	6	486	0.0184	9.40%	83.60%
8	0.0250	8.56%	71.42%	10	810	0.0237	8.63%	70.84%
12	0.0302	8.44%	68.87%	20	1620	0.0368	7.42%	57.66%
20	0.0407	8.18%	65.88%	30	2430	0.0499	6.14%	47.78%
30	0.0539	7.96%	61.56%	40	3240	0.0631	4.75%	39.89%
40	0.0670	7.58%	57.58%	50	4050	0.0762	3.29%	30.11%

Table 4: Third permeability field. Left: errors with the fixed number of offline basis  $L_i = 11$ . Right: errors with the fixed buffer number  $p_{\text{bf}} = 8$ .



## 5 Residual based online adaptive procedure

As we observe in the previous examples, the offline errors do not decrease rapidly after several multiscale functions are selected. In these cases, online basis functions can help to reduce the error and obtain an accurate approximation of the fine-scale solution [11]. The use of online basis functions gives a rapid convergence. Next, we will derive a framework for the construction of online multiscale basis functions.

We use the index  $m \geq 1$  to represent the online enrichment level. At the enrichment level  $m$ , we use  $V_{ms}^m$  to denote the corresponding space-time GMSFEM space and  $u_{ms}^m$  the corresponding solution obtained in (5). The sequence of functions  $\{u_{ms}^m\}_{m \geq 1}$  will converge to the fine-scale solution. We emphasize that the space  $V_{ms}^m$  can contain both offline and online basis functions, and define  $V_{ms}^0 = V_{\text{off}}$ . We will construct a strategy for getting the space  $V_{ms}^{m+1}$  from  $V_{ms}^m$ .

Next we present a framework for the construction of online basis functions. By online basis functions, we mean basis functions that are computed during the iterative process using the residual. This is the contrary to offline basis functions that are computed before the iterative process. The online basis functions for enrichment level  $m + 1$  are computed based on some local residuals for the multiscale solution  $u_{ms}^m$ . Thus, we see that some offline basis functions are necessary for the computations of online basis functions. In our numerical examples from the following section, we will also see how many offline basis functions are needed in order to obtain a rapidly converging sequence of solutions.

For brevity, we denote the left hand side of (5) by  $a(u_{ms}^{(n)}, v)$  and the right hand side  $F(v)$ . That is, the solution  $u_{ms} = \oplus_{n=1}^N u_{ms}^{(n)}$  where  $u_{ms}^{(n)}$  satisfies

$$a(u_{ms}^{(n)}, v) = F(v), \quad \forall v \in V_H^{(n)}.$$

Consider a given coarse neighborhood  $\omega_i$ . Suppose that at the enrichment level  $m$ , we need to add an online basis function  $\phi \in V_h$  in  $\omega_i$ . Then the required  $\phi = \oplus_{n=1}^N \phi^{(n)}$  satisfies that  $\phi^{(n)}$  is the solution of

$$a(\phi^{(n)}, v) = R^{(n)}(v), \quad \forall v \in V_h,$$

where  $R^{(n)}(v) = F(v) - a(u_{ms}^{m(n)}, v)$  is the online residual at the coarse time interval  $[T_{n-1}, T_n]$ .

In the following, we would like to form a residual based online algorithm in each coarse time interval  $[T_{n-1}, T_n]$ , see Algorithm 1. For simplicity, we will omit the time index  $(n)$  on the spaces and solutions in this description. We consider enrichment on non-overlapping coarse neighborhoods. Thus, we divide the  $\{\omega_i\}_{i=1}^{N_c}$  into  $P$  non-overlapping groups and denote each group by  $\{\omega_i\}_{i \in I_p}$ ,  $p = 1, \dots, P$ . We denote by  $M$  the number of online iterations.

---

### Algorithm 1 Residual based online algorithm

---

- 1: **Initialization:** Offline space  $V_{ms}^0 = V_{\text{off}}$ , offline solution  $u_{ms}^0 = u_H$ .
  - 2: **for**  $m = 0$  to  $M$ : **do**
  - 3:   **for**  $p = 1$  to  $P$ : **do**
  - 4:     (1) On each  $\omega_i (i \in I_p)$ , compute residual  $R^m(v) = a(u_{ms}^m, v) - F(v)$ ,  $v \in V_h$ .
  - 5:     (2) For each  $i$ , solve  $a(\phi_i, v) = R^m(v)$ ,  $\forall v \in V_h$ .
  - 6:     (3) Set  $V_{ms}^m = V_{ms}^m \cup \{\phi_i | i \in I_p\}$ .
  - 7:     (4) Solve for a new  $u_{ms}^m \in V_{ms}^m$  satisfying  $a(u_{ms}^m, v) = F(v)$ ,  $\forall v \in V_{ms}^m$ .
  - 8:   **end for**
  - 9:   Set  $V_{ms}^{m+1} = V_{ms}^m$ , and  $u_{ms}^{m+1} = u_{ms}^m$ .
  - 10: **end for**
- 

To further improve the convergence and efficiency of the online method, we can adopt an online adaptive procedure. In this adaptive approach, the online enrichment is performed for coarse neighborhoods that have a cumulative residual that is  $\theta$  fraction of the total residual. More precisely, assume that the  $V^{(n)}$  norm of local residuals on  $\{\omega_i | i \in I_p\}$ , denoted by  $\{r_i | i \in I_p\}$ , are arranged so that

$$r_{p_1} \geq r_{p_2} \geq r_{p_3} \geq \dots \geq r_{p_J},$$

where we suppose  $I_p = \{p_1, p_2, p_3, \dots, p_J\}$ . Instead of adding  $\{\phi_i | i \in I_p\}$  into  $V_{ms}^m$  at step 6 in Algorithm 1, we only add the basis  $\{\phi_1, \dots, \phi_k\}$  for the corresponding coarse neighborhoods such that  $k$  is the smallest integer satisfying

$$\sum_{i=1}^k r_{p_i}^2 \geq \theta \sum_{i=1}^J r_{p_i}^2.$$

In the examples below, we will see that the proposed adaptive procedure gives a better convergence and is more efficient.

## 6 Numerical results. Online GMsFEM

In this section, we present numerical examples to demonstrate the performance of the proposed online method in solving Equation (2). To implement the space-time online GMsFEM, we will first choose a fixed number of offline basis functions for every coarse neighborhood, and calculate the resulting offline space  $V_{\text{off}}$ . Then we conduct the online process by following Algorithm 1. In this experiment, we use the same space-time domain and mesh (coarse and fine), the same source term  $f$  and initial condition  $\beta(x, y)$ , the same definitions of relative errors  $e_1$  and  $e_2$ , as in Section 4. The permeability field  $\kappa(x, t)$  is chosen as the high-contrast permeability field 1 from Section 4.1. The buffer number in the computation of snapshot space is chosen to be 8.

First, we implement the space-time online GMsFEM by choosing different numbers of offline basis functions ( $L_i = 1, 2, 3, 4, 5$ ) on every coarse neighborhood. The relative errors of online solutions are presented in Table 5 and Table 6. Note that in the first column, we show the number of basis functions used for each coarse neighborhood  $\omega_i$ , and the degrees of freedom (DOF) of multiscale space on each coarse time interval which are the numbers in parentheses, after online enrichment. For example, 2(162) in the first column means that after online enrichment, 2 multiscale basis are used on each  $\omega_i$  and the DOF of multiscale space on each coarse time interval is 162. And if we initially choose  $L_i = 1$ , then it means 1 online iteration is performed, which add 1 online basis to each  $\omega_i$ . If  $L_i = 2$  initially, then it means we do not perform any online iteration and 2 multiscale basis are offline basis functions. By observing each column, one can see that the errors decay fast with more online iterations being performed. This is observed for both  $e_1$  and  $e_2$  when  $L_i \geq 4$ . This suggests that in this specific setting, we can get a fast online convergence with 4 offline basis chosen on each  $\omega_i$ . After a small number of online iterations, the relative errors decrease to a significantly small level. We consider reducing the high contrast of the permeability field  $\kappa(x, t)$  from  $10^6$  to 100. Then we look at the relative errors of online multiscale solutions (see Table 7 and Table 8). The same phenomena can be observed except that the fast online convergence rate can be achieved for any choice of  $L_i$ . This implies that the number of offline basis functions used to guarantee a fast online convergence rate is related to the high contrast of the permeability field.

$DOF$	$e_1(L_i = 1)$	$e_1(L_i = 2)$	$e_1(L_i = 3)$	$e_1(L_i = 4)$	$e_1(L_i = 5)$
1(81)	97.57%	-	-	-	-
2(162)	93.20%	96.71%	-	-	-
3(243)	44.24%	23.22%	21.27%	-	-
4(324)	15.37%	6.53%	7.17e-1%	10.20%	-
5(405)	8.65%	3.69%	2.06e-1%	2.58e-1%	5.20%
6(486)	5.15%	1.71%	5.41e-2%	1.75e-2%	1.06e-1%
7(567)	2.58%	3.11e-1%	5.54e-3%	6.12e-4%	2.99e-3%

Table 5: Relative online errors  $e_1$ , with the different numbers of offline basis functions. High contrast =  $10^6$ .

$DOF$	$e_2(L_i = 1)$	$e_2(L_i = 2)$	$e_2(L_i = 3)$	$e_2(L_i = 4)$	$e_2(L_i = 5)$
1(81)	138%	-	-	-	-
2(162)	113%	114%	-	-	-
3(243)	84.93%	139%	104%	-	-
4(324)	82.48%	82.08%	11.43%	73.50%	-
5(405)	69.15%	51.13%	3.29%	4.78%	48.26%
6(486)	51.17%	34.00%	1.01%	3.53e-1%	1.86%
7(567)	37.93%	7.81%	1.05e-1%	9.89e-3%	4.75e-2%

Table 6: Relative online errors  $e_2$ , with the different numbers of offline basis functions. High contrast =  $10^6$ .

$DOF$	$e_1(1 \text{ basis})$	$e_1(2 \text{ basis})$	$e_1(3 \text{ basis})$	$e_1(4 \text{ basis})$	$e_1(5 \text{ basis})$
1(81)	19.28%	-	-	-	-
2(162)	1.97%	13.03%	-	-	-
3(243)	2.81e-1%	9.81e-1%	9.27%	-	-
4(324)	3.48e-2%	1.24e-1%	2.23e-1%	8.34%	-
5(405)	1.89e-3%	1.11e-2%	9.70e-2%	2.09e-1%	7.38%
6(486)	2.67e-5%	1.33e-4%	2.07e-4%	8.71e-3%	1.56e-1%
7(567)	2.51e-7%	9.32e-7%	1.45e-6%	1.16e-4%	8.62e-3%

Table 7: Relative online errors  $e_1$ , with the different numbers of offline basis functions. High contrast = 100.

$DOF$	$e_2(1 \text{ basis})$	$e_2(2 \text{ basis})$	$e_2(3 \text{ basis})$	$e_2(4 \text{ basis})$	$e_2(5 \text{ basis})$
1(81)	219%	-	-	-	-
2(162)	14.75%	123%	-	-	-
3(243)	3.35%	8.37%	81.80%	-	-
4(324)	4.03e-1%	1.11%	2.63%	67.86%	-
5(405)	2.11e-2%	1.01e-1%	1.68e-1%	2.29%	59.93%
6(486)	5.61e-4%	1.64e-3%	3.71e-3%	1.35e-1%	1.77%
7(567)	4.57e-6%	1.72e-5%	2.29e-5%	2.08e-3%	1.41e-1%

Table 8: Relative online errors  $e_2$  with the different numbers of offline basis functions. High contrast = 100.

Next, we perform online adaptive basis construction procedure with  $\theta = 0.7$ . The numerical results for using 3, 4, and 5 offline basis per coarse neighborhood are shown in Table 9. Notice that "M1 + M2" in the DOF columns means M1 degrees of freedom are used on the first coarse time interval and M2 degrees of freedom on the second coarse time interval. To compare the behaviors of online processes with and without adaptivity, we plot out the log values of  $e_2$  against DOFs. See Figure 6. We observe that to achieve a certain error, fewer online basis functions are needed with adaptivity. This indicates that the proposed adaptive procedure gives us better convergence and is more efficient.

3 offline basis		4 offline basis		5 offline basis	
DOF	$e_2$	DOF	$e_2$	DOF	$e_2$
243+243	104%	324+324	73.50%	405+405	48.26%
323+322	10.57%	399+401	3.56%	471+473	1.95%
403+392	1.49%	468+466	2.13e-1%	533+536	1.21e-1%
480+465	9.81e-2%	541+529	1.03e-2%	599+603	6.81e-3%
552+533	4.24e-3%	611+601	5.00e-4%	670+669	3.41e-4%

Table 9: Relative online adaptive errors  $e_2$  with different numbers of offline basis functions.

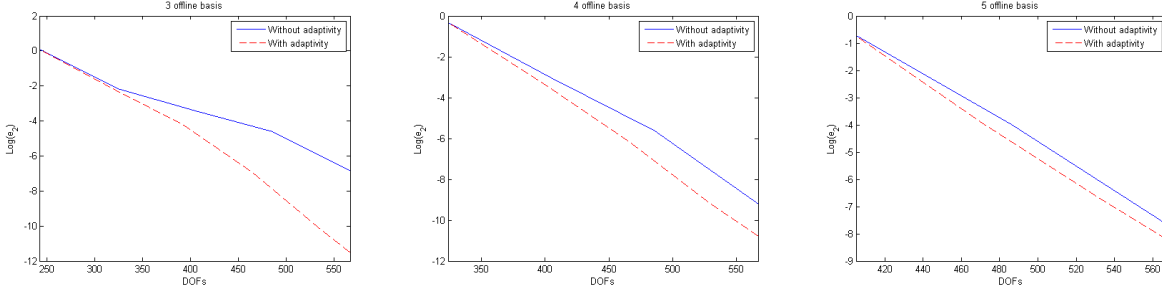


Figure 6: Adaptivity v.s. no adaptivity.

## 7 Conclusion

In this paper, we consider the construction of the space-time GMsFEM to solve space-time heterogeneous parabolic equations. The main ingredients of our approach are (1) the construction of space-time snapshot vectors, (2) the local spectral decomposition in the snapshot space. To construct the snapshot vectors, we solve local problems in local space-time domains. A complete snapshot space will consist of the use of all possible boundary and initial conditions. However, this can result to very large computational cost and a high dimensional snapshot space. For this reason, we compute a number of randomized snapshot vectors. In fact, the number of snapshot vectors is slightly larger than that of the multiscale basis functions used in the simulations. To perform local spectral decomposition, we discuss a couple of choices for local eigenvalue problems motivated by the analysis. We present a convergence analysis of the proposed method. Several numerical examples are presented. In particular, we consider examples where the space-time permeability fields have high contrast and these high-conductivity regions move in the space. If only spatial multiscale basis functions are used, it will require a large dimensional space. Thanks to the space-time multiscale space, we can approximate the problem with a fewer degrees of freedom. Our numerical results show that one can obtain accurate solutions. We also discuss online procedures, where new multiscale basis functions are constructed using the residual. These basis functions are computed in each local space-time domain. Using online basis functions adaptively, one can reduce the error substantially at a cost of online computations.

In this paper, our main objective is to develop systematic multiscale model reduction techniques in space-time cells by constructing local (in space-time) multiscale basis functions. The proposed concepts can be used for other applications, where one needs space-time multiscale basis functions.

## 8 Appendix

### 8.1 Proof of Lemma 3.1

*Proof.* By the definition of  $\|\cdot\|_{V^{(n)}}$ ,

$$\begin{aligned}
\|u_h - u_H\|_{V^{(n)}}^2 &= \frac{1}{2} \int_{\Omega} (u_h - u_H)^2|_{t=T_n^-} + \frac{1}{2} \int_{\Omega} (u_h - u_H)^2|_{t=T_{n-1}^+} + \int_{T_{n-1}}^{T_n} \int_{\Omega} \kappa |\nabla(u_h - u_H)|^2 \\
&= \frac{1}{2} \int_{T_{n-1}}^{T_n} \int_{\Omega} \frac{\partial}{\partial t} (u_h - u_H)^2 + \int_{\Omega} (u_h - u_H)^2|_{t=T_{n-1}^+} + \int_{T_{n-1}}^{T_n} \int_{\Omega} \kappa |\nabla(u_h - u_H)|^2 \\
&= \int_{T_{n-1}}^{T_n} \int_{\Omega} \frac{\partial(u_h - u_H)}{\partial t} (u_h - u_H) + \int_{\Omega} (u_h - u_H)^2|_{t=T_{n-1}^+} \\
&\quad + \int_{T_{n-1}}^{T_n} \int_{\Omega} \kappa |\nabla(u_h - u_H)|^2 \\
&= \int_{T_{n-1}}^{T_n} \int_{\Omega} \frac{\partial(u_h - u_H)}{\partial t} (u_h - w) + \int_{\Omega} (u_h - u_H)(u_h - w)|_{t=T_{n-1}^+} \\
&\quad + \int_{T_{n-1}}^{T_n} \int_{\Omega} \kappa \nabla(u_h - u_H) \cdot \nabla(u_h - w) + \int_{T_{n-1}}^{T_n} \int_{\Omega} \frac{\partial(u_h - u_H)}{\partial t} (w - u_H) \\
&\quad + \int_{\Omega} (u_h - u_H)(w - u_H)|_{t=T_{n-1}^+} + \int_{T_{n-1}}^{T_n} \int_{\Omega} \kappa \nabla(u_h - u_H) \cdot \nabla(w - u_H). \tag{29}
\end{aligned}$$

From (5) and the similar formulation for fine scale solution  $u_h$ , we have

$$\begin{aligned}
&\int_{T_{n-1}}^{T_n} \int_{\Omega} \frac{\partial(u_h - u_H)}{\partial t} v + \int_{T_{n-1}}^{T_n} \int_{\Omega} \kappa \nabla(u_h - u_H) \cdot \nabla v + \int_{\Omega} (u_h - u_H)v|_{t=T_{n-1}^+} \\
&= \int_{\Omega} \left( g_h^{(n)} - g_H^{(n)} \right) v(x, T_{n-1}^+), \quad \forall v \in V_H^{(n)}. \tag{30}
\end{aligned}$$

Therefore, taking  $v = w - u_H$  and combining the equation (29) and (30), we obtain

$$\begin{aligned}
\|u_h - u_H\|_{V^{(n)}}^2 &= \int_{T_{n-1}}^{T_n} \int_{\Omega} \frac{\partial(u_h - u_H)}{\partial t} (u_h - w) + \int_{\Omega} (u_h - u_H)(u_h - w)|_{t=T_{n-1}^+} \\
&\quad + \int_{T_{n-1}}^{T_n} \int_{\Omega} \kappa \nabla(u_h - u_H) \cdot \nabla(u_h - w) + \int_{\Omega} \left( g_h^{(n)} - g_H^{(n)} \right) (w - u_H)|_{t=T_{n-1}^+}.
\end{aligned}$$

Using integration by parts, we have

$$\begin{aligned}
&\int_{T_{n-1}}^{T_n} \int_{\Omega} \frac{\partial(u_h - u_H)}{\partial t} (u_h - w) + \int_{\Omega} (u_h - u_H)(u_h - w)|_{t=T_{n-1}^+} \\
&= - \int_{T_{n-1}}^{T_n} \int_{\Omega} \frac{\partial(u_h - w)}{\partial t} (u_h - u_H) + \int_{\Omega} (u_h - u_H)(u_h - w)|_{t=T_n^-}.
\end{aligned}$$

Thus,

$$\begin{aligned}
\|u_h - u_H\|_{V^{(n)}}^2 &= - \int_{T_{n-1}}^{T_n} \int_{\Omega} \frac{\partial(u_h - w)}{\partial t} (u_h - u_H) + \int_{\Omega} (u_h - u_H)(u_h - w)|_{t=T_n^-} \\
&\quad + \int_{T_{n-1}}^{T_n} \int_{\Omega} \kappa \nabla(u_h - u_H) \cdot \nabla(u_h - w) + \int_{\Omega} (g_h^{(n)} - g_H^{(n)}) (u_h - u_H)|_{t=T_{n-1}^+} \\
&\quad + \int_{\Omega} (g_h^{(n)} - g_H^{(n)}) (w - u_h)|_{t=T_{n-1}^+} \\
&\leq C \left\| \frac{\partial(u_h - w)}{\partial t} \right\|_{L^2((T_{n-1}, T_n); H^{-1}(\kappa))} \|u_h - u_H\|_{L^2((T_{n-1}, T_n); \kappa)} \\
&\quad + \|(u_h - u_H)(\cdot, T_n^-)\|_{L^2(\Omega)} \|(u_h - w)(\cdot, T_n^-)\|_{L^2(\Omega)} \\
&\quad + \|u_h - w\|_{L^2((T_{n-1}, T_n); \kappa)} \|u_h - u_H\|_{L^2((T_{n-1}, T_n); \kappa)} \\
&\quad + \|g_h^{(n)} - g_H^{(n)}\|_{L^2(\Omega)} (\|(u_h - u_H)(\cdot, T_{n-1}^+)\|_{L^2(\Omega)} \\
&\quad + \|(u_h - w)(\cdot, T_{n-1}^+)\|_{L^2(\Omega)}).
\end{aligned}$$

Using Young's inequality, we have

$$\|u_h - u_H\|_{V^{(n)}}^2 \leq \frac{1}{2} \|u_h - u_H\|_{V^{(n)}}^2 + 2 \left( C \|u_h - w\|_{W^{(n)}}^2 + \|g_h^{(n)} - g_H^{(n)}\|_{L^2(\Omega)}^2 \right).$$

and

$$\begin{aligned}
\|g_h^{(n)} - g_H^{(n)}\|_{L^2(\Omega)}^2 &= \begin{cases} 0 & \text{for } n = 1 \\ \|u_h^{(n-1)}(\cdot, T_{n-1}^-) - u_H^{(n-1)}(\cdot, T_{n-1}^-)\|_{L^2(\Omega)}^2 & \text{for } n > 1 \end{cases} \\
&\leq \begin{cases} 0 & \text{for } n = 1 \\ \|u_h - u_H\|_{V^{(n-1)}}^2 & \text{for } n > 1 \end{cases}.
\end{aligned}$$

Therefore, we proved the lemma. □

## References

- [1] Assyr Abdulle and Martin Ernst Huber. Finite element heterogeneous multiscale method for nonlinear monotone parabolic homogenization problems. Technical report, 2014.
- [2] Lawrence Bush, Victor Ginting, and Michael Presho. Application of a conservative, generalized multiscale finite element method to flow models. *Journal of Computational and Applied Mathematics*, 260:395–409, 2014.
- [3] V. Calo, Y. Efendiev, J. Galvis, and G. Li. Randomized oversampling for generalized multiscale finite element methods. <http://arxiv.org/pdf/1409.7114.pdf>, 2014.
- [4] Victor M Calo, Yalchin Efendiev, Juan Galvis, and Guanglian Li. Randomized oversampling for generalized multiscale finite element methods. *arXiv preprint arXiv:1409.7114*, 2014.
- [5] Ho Yuen Chan, Eric T Chung, and Yalchin Efendiev. Adaptive mixed gmsfem for flows in heterogeneous media. *arXiv preprint arXiv:1507.01659*, 2015.
- [6] E. Chung and Y. Efendiev. Reduced-contrast approximations for high-contrast multiscale flow problems. *SIAM J. Multiscale Modeling and Simulation*, 8:1128–1153, 2010.

- [7] E Chung and Wing Tat Leung. A sub-grid structure enhanced discontinuous galerkin method for multiscale diffusion and convection-diffusion problems. *Comput. Phys*, 14:370–392, 2013.
- [8] Eric T Chung, Yalchin Efendiev, and Shubin Fu. Generalized multiscale finite element method for elasticity equations. *GEM-International Journal on Geomathematics*, 5(2):225–254, 2014.
- [9] Eric T Chung, Yalchin Efendiev, and Wing Tat Leung. An online generalized multiscale discontinuous galerkin method (gmsdgm) for flows in heterogeneous media. *arXiv preprint arXiv:1504.04417*, 2015.
- [10] Eric T Chung, Yalchin Efendiev, and Wing Tat Leung. Residual-driven online generalized multiscale finite element methods. *arXiv preprint arXiv:1501.04565*, 2015.
- [11] Eric T. Chung, Yalchin Efendiev, and Wing Tat Leung. Residual-driven online generalized multiscale finite element methods. *J. Comput. Phys.*, 302(C):176–190, December 2015.
- [12] Eric T Chung, Yalchin Efendiev, Guanglian Li, and Maria Vasilyeva. Generalized multiscale finite element methods for problems in perforated heterogeneous domains. *Applicable Analysis*, to appear, 2015.
- [13] E.T. Chung, Y. Efendiev, and W.T. Leung. An adaptive generalized multiscale discontinuous galerkin method (gmsdgm) for high-contrast flow problems. submitted to SIAM MMS.
- [14] E.T. Chung, Y. Efendiev, and W.T. Leung. Generalized multiscale finite element method for wave propagation in heterogeneous media. to appear in SIAM MMS.
- [15] E.T. Chung, Y. Efendiev, and G. Li. An adaptive GMsFEM for high-contrast flow problems. *Journal of Computational Physics*, 273:54–76, 2014.
- [16] Y. Efendiev, J. Galvis, and T. Hou. Generalized multiscale finite element methods. *Journal of Computational Physics*, 251:116–135, 2013.
- [17] Y. Efendiev, J. Galvis, R. Lazarov, and J. Willems. Robust domain decomposition preconditioners for abstract symmetric positive definite bilinear forms. *ESAIM Math. Model. Numer. Anal.*, 46(5):1175–1199, 2012.
- [18] Y. Efendiev, J. Galvis, and P.S. Vassilevski. Spectral element agglomerate algebraic multigrid methods for elliptic problems with high-contrast coefficients. In *Domain decomposition methods in science and engineering XIX*, volume 78 of *Lect. Notes Comput. Sci. Eng.*, pages 407–414. Springer, Heidelberg, 2011.
- [19] Y. Efendiev and T. Hou. *Multiscale Finite Element Methods: Theory and Applications*. Springer, 2009.
- [20] Y Efendiev and A Pankov. Numerical homogenization of nonlinear random parabolic operators. *Multiscale Modeling & Simulation*, 2(2):237–268, 2004.
- [21] Y Efendiev, A Pankov, et al. Homogenization of nonlinear random parabolic operators. *Advances in Differential Equations*, 10(11):1235–1260, 2005.
- [22] Yalchin Efendiev, Juan Galvis, R Lazarov, M Moon, and Marcus Sarkis. Generalized multiscale finite element method. symmetric interior penalty coupling. *Journal of Computational Physics*, 255:1–15, 2013.
- [23] Jacob Fish and Wen Chen. Space–time multiscale model for wave propagation in heterogeneous media. *Computer Methods in applied mechanics and engineering*, 193(45):4837–4856, 2004.
- [24] T. Hou and X.H. Wu. A multiscale finite element method for elliptic problems in composite materials and porous media. *J. Comput. Phys.*, 134:169–189, 1997.

- [25] Thomas JR Hughes and James R Stewart. A space-time formulation for multiscale phenomena. *Journal of Computational and Applied Mathematics*, 74(1):217–229, 1996.
- [26] Vasilii Vasil’evich Jikov, Sergei M Kozlov, and Olga Arsen’evna Oleinik. *Homogenization of differential operators and integral functionals*. Springer Science & Business Media, 2012.
- [27] Rouven Künze and Ivan Lunati. An adaptive multiscale method for density-driven instabilities. *Journal of Computational Physics*, 231(17):5557–5570, 2012.
- [28] Arif Masud and Thomas JR Hughes. A space-time galerkin/least-squares finite element formulation of the navier-stokes equations for moving domain problems. *Computer Methods in Applied Mechanics and Engineering*, 146(1):91–126, 1997.
- [29] Pingbing Ming and Pingwen Zhang. Analysis of the heterogeneous multiscale method for parabolic homogenization problems. *Mathematics of Computation*, 76(257):153–177, 2007.
- [30] H Nguyen and J Reynen. A space-time least-square finite element scheme for advection-diffusion equations. *Computer Methods in Applied Mechanics and Engineering*, 42(3):331–342, 1984.
- [31] Houman Owhadi and Lei Zhang. Homogenization of parabolic equations with a continuum of space and time scales. *SIAM Journal on Numerical Analysis*, 46(1):1–36, 2007.
- [32] Aleksandr Andreevich Pankov. *G-convergence and homogenization of nonlinear partial differential operators*, volume 422. Springer Science & Business Media, 2013.
- [33] Grigorios A Pavliotis and Andrew Stuart. *Multiscale methods: averaging and homogenization*. Springer Science & Business Media, 2008.
- [34] Kenji Takizawa and Tayfun E Tezduyar. Multiscale space–time fluid–structure interaction techniques. *Computational Mechanics*, 48(3):247–267, 2011.
- [35] Tayfun E Tezduyar, M Behr, S Mittal, and AA Johnson. Computation of unsteady incompressible flows with the stabilized finite element methods: space-time formulations, iterative strategies and massively parallel implementations. *Asme Pressure Vessels Piping Div Publ PVP*, 246:7–24, 1992.